

Article

Numerical Simulation Study of Gas-Liquid Two-Phase Flow in a Pressurized Leaching Stirred Tank

Zhongzheng Zhao ^{1,2}, Fengyang Chen ^{1,2}, Junchang Liu ³, Qihong Liu ^{1,2}, Yanqing Hou ^{1,2,*}, Ni Yang ^{3,*} and Gang Xie ³

¹ Faculty of Metallurgical and Energy Engineering, Kunming University of Science and Technology, Kunming 650093, China; chenfengyang0315@163.com (F.C.)

² State Key Laboratory of Complex Nonferrous Metal Resources Clean Utilization, Kunming University of Science and Technology, Kunming 650093, China

³ Metallurgical and Environmental Protection Department, Kunming Metallurgical Research Institute Co., Ltd., Kunming 650093, China

* Correspondence: hhouyanqing@163.com (Y.H.); yangnihejie@126.com (N.Y.)

Abstract: The gas-liquid flow and oxygen content in a pressurized leaching stirred tank significantly influence the chemical reaction rates, while the specific dynamics of gas-liquid flow in the sulfuric acid system remain largely unexplored. In this study, a mathematical model of gas-liquid flow within a stirred tank is developed using the Euler-Euler approach, with the turbulence and drag force models being validated against experimental data. Utilizing this validated and reliable model, this study investigates the impacts of the sulfuric acid concentration, baffles, air inlet velocity, and bubble diameter on the flow field and gas holdup in a two-phase system consisting of a sulfuric acid solution and oxygen. The findings indicate that introducing a specific concentration of sulfuric acid decreases the solution velocity and increases the gas holdup within the tank. However, once the sulfuric acid concentration reaches a certain threshold, further increases have a diminished effect on the gas-liquid phases. The installation of baffles enhances the turbulent kinetic energy and increases the gas holdup while only resulting in a minimal 1.2% increase in power consumption. Additionally, the inlet velocity and bubble diameter have a relatively minor impact on the tank's flow field. However, increasing the inlet velocity significantly boosts the gas holdup, whereas an increase in the bubble diameter marginally reduces it. Furthermore, introducing a sulfuric acid solution into the tank can enhance the gas holdup when the gas inlet velocity is low. Conversely, when the gas inlet velocity is high, the addition of sulfuric acid results in a decrease in the gas holdup. The conclusions from this study contribute to enhancing the mixing effectiveness and oxygen content within the tank, providing a substantial theoretical basis for optimizing the design and operating conditions of pressurized leaching stirred tanks.

Keywords: stirred tank; flow field; gas holdup; numerical simulation; gas-liquid two-phase flow



Citation: Zhao, Z.; Chen, F.; Liu, J.; Liu, Q.; Hou, Y.; Yang, N.; Xie, G. Numerical Simulation Study of Gas-Liquid Two-Phase Flow in a Pressurized Leaching Stirred Tank. *Processes* **2024**, *12*, 896. <https://doi.org/10.3390/pr12050896>

Academic Editor: Krzysztof Rogowski

Received: 12 March 2024

Revised: 12 April 2024

Accepted: 23 April 2024

Published: 28 April 2024



Copyright: © 2024 by the authors. Licensee MDPI, Basel, Switzerland. This article is an open access article distributed under the terms and conditions of the Creative Commons Attribution (CC BY) license (<https://creativecommons.org/licenses/by/4.0/>).

1. Introduction

Pressurized hydrometallurgy increases the efficiency of the metallurgical reaction process by elevating the gas phase pressure, enhancing the mass transfer process in the gas phase, and raising the reaction temperature of the system to augment the driving force of the chemical reaction. This technique is extensively used in the leaching of non-ferrous metals and the comprehensive recycling of rare and precious metals, owing to its wide adaptability of raw materials, superior reaction efficiency, and minimal environmental pollution [1,2]. The stirred tank is the leading equipment in hydrometallurgy. In the general leaching process, oxygen as an oxidant is passed into the stirred tank. Under the action of stirring, it is dispersed to the stirred tank everywhere in order to better participate in the reaction, and the solution is in the rotating action of the impeller in the stirred tank circulating flow. This pressurized leaching process is an oxygen-consuming system where

the oxygen content in the solution plays a crucial role in determining the chemical reaction rate in the stirred tank. Enhancing the oxygen content facilitates an increase in the gas-liquid contact area and accelerates the mass transfer rate between the gas-liquid phases. Good liquid flow circulation in the stirred tank can accelerate the gas-liquid-solid reaction process and promote the reaction [3–6]. Consequently, conducting an in-depth study of the gas-liquid two-phase flow field and gas holdup in stirred tanks holds significant importance for industrial production.

The flow field in a pressurized stirred tank constitutes a complex, stochastic, turbulent, and multiphase flow. Simultaneously, the high temperature and high-pressure operating conditions of the pressurized stirred tank present significant challenges to the experimental measurement of the flow field [7]. Presently, the mainstream methods for flow field detection are laser Doppler velocimetry (LDV) and particle image velocimetry (PIV) [8,9]. These detection methods have less impact on the flow field and can obtain more accurate flow information. However, when applied to large mixing equipment, it takes a long time, the measurement equipment is expensive, and it is not easy to obtain accurate data for complex production processes. Computational fluid dynamics (CFD) has emerged as a type of technology for overcoming challenges in fluid flow research by constructing flow field models and importing the flow field parameters into computers. This approach enables the prediction and real-time visualization of flow fields, allowing for the acquisition of microscopic information that is difficult to obtain through traditional experimental methods. Such information includes the turbulent energy and dissipation rates in the flow field. Additionally, numerical simulations with CFD can reduce the number of required experiments, thereby lowering the costs associated with flow field research. It has become a commonly used method in optimizing equipment design [10,11].

Zhang et al. [12] introduced a modification to the standard turbulence model, utilizing the number of spins to enhance the accuracy of numerical simulations of the gas-liquid flow in stirred tanks. Wang et al. [13] analyzed the gas-liquid dispersion characteristics of different impeller combinations by using the CFD method, verified it with PIV experiments, and analyzed the distribution of the gas holdup under different operating conditions. The results showed that the gas holdup around the impeller increased significantly, and the bubble size was more homogeneous when using the upper six-blade skewed propeller and the lower six-blade curved turbine propeller. Chieng et al. [14] employed simulation software to investigate the effects of different impeller installation positions on the flow field and solid-liquid suspension characteristics inside the stirred tank. The results demonstrated that the flow field transitioned from a typical double-loop structure to a single-loop one, accompanied by an increase in axial flow and a reduction in mixing time when the Rushton impeller position was lower. Heidari et al. [15] explored the effect of the impeller tilt angle on stirring and mixing in stirred tanks, concluding that an impeller tilt of 30 °C yields the best results. Hosseini et al. [16] compared various impellers and optimized the blade thickness, disc width, and vertical angle of the impeller via the response surface method. Chen et al. [17] investigated the gas-liquid two-phase flow in a stirred tank using the Euler multiphase flow model, and the results showed that increasing the rotational speed is favorable for gas-phase distribution and liquid-phase mixing, and increasing the height of the impeller from the bottom can increase the gas holdup. Naeeni et al. [18] simulated the flow field in a stirred tank in the two-phase regime of oil and water, and the results showed a decrease in bubble diameter with an increasing rotational speed and a concomitant improvement in the homogeneity of the system. Li et al. [19] simulated gas-liquid dispersion in a stirred tank with low and high gas loads using a PBM model in the water and air regime, and the results showed that a two-loop flow pattern was formed in the stirred tank at high gas loads, and a three-loop flow pattern was formed in the stirred tank at low loads. Appa et al. [20] simulated the flow field, gas-phase diffusion, and bubble size inside the autoclave in an air-water two-phase regime and compared the experimental and simulation results with the PIV method. The results showed that the flow field inside the autoclave was a double-loop structure, the jet at the paddle was at a certain

angle to the horizontal direction, the inclination angle was related to the rotational speed, and the Euler-Euler model provided accurate prediction of the gas-phase distribution and bubble size.

Currently, research on gas-liquid two-phase flow in stirred tanks primarily concentrates on optimizing equipment conditions, such as for the stirring paddle, and examining the distribution of gas-liquid flow within the tank under fixed conditions, with water and air often serving as the operating medium. However, there have been limited investigations of the effects of changes in the inlet conditions and fluid properties, especially under sulfuric acid and two-phase water conditions, on the characteristics of gas-liquid flow within stirred tanks.

This paper employs CFD technology to conduct a numerical simulation of the gas-liquid two-phase flow in a pressurized leaching stirred tank, confirms the reliability of the simulation with experimental data, and explores the influence of the sulfuric acid concentration, baffle plate, air inlet speed, and bubble diameter on the gas-liquid flow in a stirred tank to furnish a detailed technical foundation for the optimal design of the stirred tank.

2. CFD Model Details

2.1. Physical Model

The model developed was a six-blade standard Rushton impeller stirred tank with a baffle [21]. The stirred tank was a cylinder with a bottom diameter equal to the height of the tank with the specific data $L = H = 288$ mm, and the baffle was of the same height as the stirred tank. It had a width of $H/10$, and the baffle was given a no-thickness wall treatment to simplify the computational conditions. The gas entered the stirred tank through a circular gas distributor directly below the impeller, with a ring width of $N = 77$ mm and a distance from the impeller of $B = 35$ mm. The Rushton impeller had a diameter of $A = 96$ mm, a height of $H/3$ from the bottom, an impeller width of $0.25 A$, a height of $W = 0.2 A$, and a paddle disk diameter of $0.75 A$. The model was built using the industrial 3D modeling software SolidWorks 2022, and the schematic diagram of its generated computational domain and geometric model is shown in Figure 1.

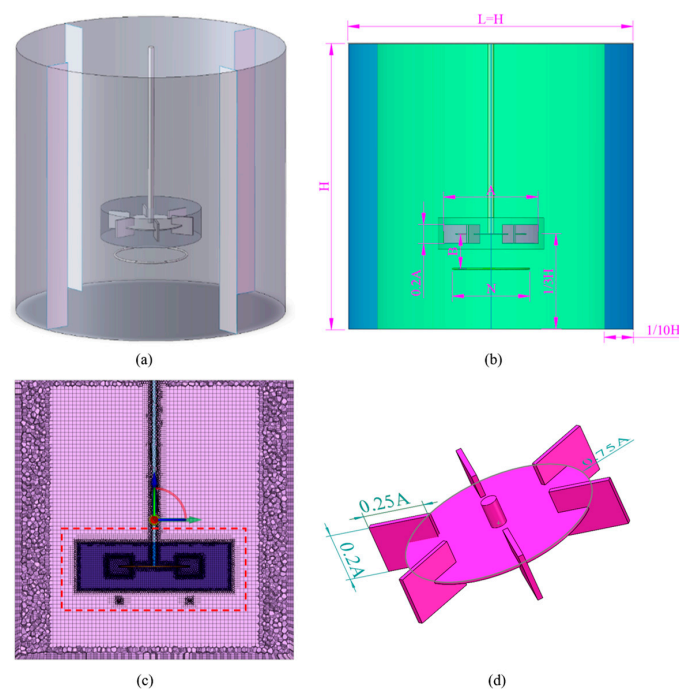


Figure 1. (a) Computational domain. (b) Schematic diagram of the stirred tank. (c) Structured grid. (d) Rushton turbine.

This study employed Fluent 14.5 Meshing software to mesh the geometric model using a poly-hexcore mesh type. Figure 2 displays two distinct types of mesh cells: hexcore and polyhedral. In the solution process, the use of hexcore mesh is superior to poly mesh because the computational accuracy of the hexcore mesh will be a little bit higher, but its mesh delineation is more difficult, which easily leads to poor quality for the mesh, whereas the polyhedra mesh delineation is relatively simple and is suitable for dealing with complex geometric regions [22]. The poly-hexcore mesh type adopts a hybrid meshing scheme, which enables hexahedral and polyhedral meshes to realize co-nodal connections, and it adopts hexcore meshing in the core region of the solution and polyhedra meshing in the wall and transition region, which fully combines the advantages of polyhedra meshing and hexcore meshing, effectively improving the quality of the mesh while reducing the number of meshes and reducing the amount of computation [23].

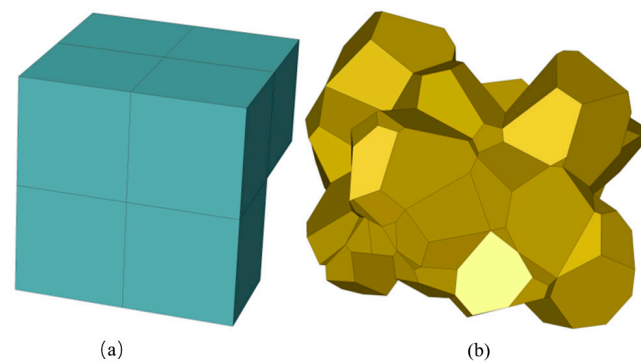


Figure 2. (a) Hexcore. (b) Polyhedral.

The multiple reference frame (MRF) method was utilized to treat the stirred region within the stirred tank [24]. Owing to its simplicity and calculation accuracy without the need for repeated iterations, the MRF method enjoys widespread use in research. Its principle involves dividing the stirred tank into an internal dynamic region featuring an impeller and an external static region and establishing an intersection surface in the middle for data exchange. Within the dynamic region, the working conditions become more complex due to the impeller's rotation. Thus, the mesh is locally refined to enhance the result's accuracy and calculation convergence. This local refinement effectively improves the mesh quality while preventing rapid increases in mesh count, thereby enhancing the efficiency of the calculations.

2.2. Governing Equations

In this paper, the Euler-Euler two-phase flow model is used to describe the gas-liquid two-phase flow in the stirred tank, and its continuity equation can be expressed as follows:

$$\frac{\partial(\rho_g \alpha_g)}{\partial t} + \nabla \cdot (\rho_g \times \alpha_g \times u_g) = 0 \quad (1)$$

$$\frac{\partial(\rho_l \alpha_l)}{\partial t} + \nabla \cdot (\rho_l \times \alpha_l \times u_l) = 0 \quad (2)$$

where α_g , ρ_g , and u_g are the gas-phase volume fraction, density, and flow rate, respectively, α_l , ρ_l , and u_l are the liquid-phase volume fraction, density, and flow rate, respectively, and t is time.

In the Eulerian two-fluid model, the sum of the volume fractions of the gas and liquid phases is one such that

$$\alpha_g + \alpha_l = 1 \quad (3)$$

The momentum equation can be expressed as follows:

$$\frac{\partial(\rho_g \alpha_g u_g)}{\partial t} + \nabla \cdot (\rho_g \times \alpha_g \times u_g \times u_g) - \alpha_g \nabla p + \nabla \cdot (\alpha_g \mu_{eff,g} (\nabla u_g + (\nabla u_g)^T)) + \alpha_g \rho_g g + I_{g,l} \quad (4)$$

$$\frac{\partial(\rho_l \alpha_l u_l)}{\partial t} + \nabla \cdot (\rho_l \times \alpha_l \times u_l \times u_l) - \alpha_l \nabla p + \nabla \cdot (\alpha_l \mu_{eff,l} (\nabla u_l + (\nabla u_l)^T)) + \alpha_l \rho_l g + I_{l,g} \quad (5)$$

where ρ is the density, p is the pressure, μ_{eff} is the effective viscosity, $\mu_{eff} = \mu_{mol} + \mu_{turb}$, μ_{mol} is the molecular viscosity, μ_{turb} is the turbulence viscosity, u is the velocity vector, and g is the gravitational acceleration. Meanwhile, $I_{g,l}$, $I_{l,g}$ are the gas-liquid inter-phase forces. Khopkar et al. [25] employed the Euler-Euler model to simulate the gas-liquid flow within a stirred tank and ascertained that, compared with the drag, the influences of the added mass force and lift force were inconsequential. In a parallel vein, Ljungqvist et al. [26] arrived at a similar conclusion, identifying the drag force as the predominant interphase interaction force, with the added mass force, lift force, and turbulent diffusion force exerting minimal impact on the calculated slip velocity. Furthermore, Sanyal and Lane [27,28] also concluded that when compared with the drag, other interphase forces could be disregarded. Consequently, in the present study, only the drag force is considered for the interphase interaction forces.

The Reynolds time-averaged standard $k - \epsilon$ model is used for the turbulence equations to describe the gas-liquid two-phase turbulent flow in the stirred tank. The $k - \epsilon$ model is a semiempirical model based on the transport equations for the turbulence kinetic energy (k) and the turbulence dissipation rate (ϵ), which have been widely applied to practical engineering fluid calculations with reasonable accuracy and economy [29]. Jaworski et al. [30] employed six turbulence models, encompassing the standard $k - \epsilon$, realizable, and RNG models, to simulate a baffled slant-blade turboprop stirred tank. They juxtaposed the simulation outcomes with experimental data obtained via LDA in the jet region adjacent to the stirred tank's wall. The findings indicated that the standard $k - \epsilon$ model excels in forecasting the axially averaged velocity components. Regarding the turbulent kinetic energy distribution, while all models yielded predictions marginally lower than what was observed, the standard model's estimates were nearest to the experimental measurements.

Here, the k equation is derived from the exact equation

$$\frac{\partial}{\partial x_i} (\rho u_i k) = \frac{\partial}{\partial x_j} \left(\left(\mu + \frac{\mu_t}{\sigma_k} \right) \frac{\partial k}{\partial x_j} \right) - \frac{\partial}{\partial t} (\rho k) + G_k + G_b - \rho \epsilon \quad (6)$$

The ϵ equation is obtained by physical reasoning:

$$\frac{\partial}{\partial x_i} (\rho u_i \epsilon) = \frac{\partial}{\partial x_j} \left(\left(\mu + \frac{\mu_t}{\sigma_\epsilon} \right) \frac{\partial \epsilon}{\partial x_j} \right) - \frac{\partial}{\partial t} (\rho \epsilon) + C_{1\epsilon} \frac{\epsilon}{k} (G_k + C_{3\epsilon} G_b) - C_{2\epsilon} \rho \frac{\epsilon^2}{k} \quad (7)$$

where the turbulent viscosity μ_t is calculated using ϵ and k :

$$\mu_t = \rho C_\mu \frac{k^2}{\epsilon} \quad (8)$$

where G_k denotes the turbulent kinetic energy generated by the mean velocity gradient and G_b denotes the turbulent kinetic energy generated by buoyancy. $C_{1\epsilon}$, $C_{2\epsilon}$, σ_k , σ_ϵ , and C_μ are model constants determined by basic turbulence experiments, with default values of 1.44, 1.92, 1.0, 1.3, and 0.09, respectively.

2.3. Boundary Conditions

The gas entered the stirred tank from the annular gas distributor below the impeller, using the normal phase velocity of the gas phase as the inlet condition and defining its gas-phase volume fraction as one. We set the liquid phase surface in the stirred tank as a pressure outlet. The dynamic and static area interfaces were set as the INTERFACE for exchanging flow information. The wall surface of the stirred tank adopted the no-slip boundary condition, the turbulence model adopted the widely used standard $k - \varepsilon$ model, gravity was turned on, and the steady state solution of the phase-coupled SIMPLE algorithm model solved the gas-liquid two-phase flow. All the convergence residual conditions were set to 10^{-4} .

3. Model Validation

3.1. Grid Independence

Generally, an increase in grid quantity leads to a finer division of the computational domain, enhancing computational accuracy, but this also escalates the hardware requirements, simultaneously leading to prolonged solving times and slower convergence, among other issues. The purpose of the grid independence test is to find a balance between computational accuracy and computational volume [31].

The experimental data for the experimental validation in the next section and the grid independence test in this section were taken from the work of Guan et al. [32]. Normalization of the liquid-phase velocity and axial range was achieved by defining the normalized liquid-phase velocity as U/U_{tip} , with U representing the liquid-phase velocity and U_{tip} denoting the impeller tip's linear velocity. $Z = 0$ corresponds to the midplane of the paddle disk of the Rushton impeller, W indicates the paddle's height, and S represents the radial distance from the impeller's tip.

Figure 3 demonstrates the prediction of the axial distribution of the normalized liquid-phase velocity in the discharge zone in the stirred tank for four grid number incremental meshing schemes. There was a bias in the prediction of the velocity at $2Z/W = 0$ when the number of grids was 1.4×10^5 . When the number of grid cells increased to 3.2×10^5 , the prediction of the velocity at $2Z/W = 0$ was corrected, but the prediction of the maximum velocity was small. When the number of grid cells increased to 5.2×10^5 , the prediction of the liquid-phase velocity was even closer to the experimental results, and when the number of grid cells increased to 15.7×10^5 , the axial normalized liquid-phase velocity distribution did not change much compared with that of the 5.2×10^5 grid (i.e., increasing the number of grid cells could not improve the computational accuracy effectively). Therefore, the number of grid cells in this study would finally be 5.2×10^5 after integrating the calculation accuracy and time cost.

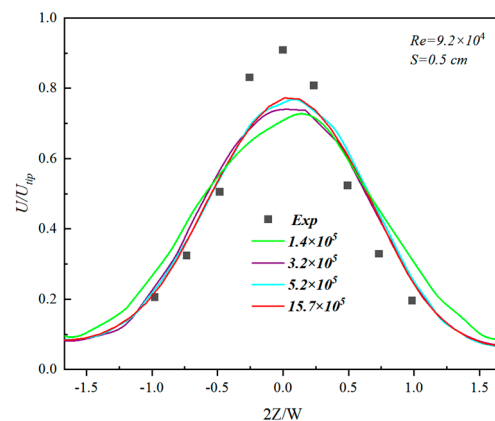


Figure 3. Grid independence study for normalized liquid velocity.

3.2. Turbulence Model Validation

Under gas-liquid biphasic conditions, the predictive capabilities of five distinct turbulence models (standard k-epsilon, RNG, SST, RSM, and realizable) were evaluated. This assessment focused on forecasting the axial distribution of the normalized liquid-phase velocity and gas holdup in the discharge area at a stirring Reynolds number of $Re = 9.2 \times 10^4$ and at distances of 0.5 cm and 5.5 cm from the tip of the stirring impeller. The purpose of this evaluation was to verify the selection of turbulence models for accurately predicting the flow dynamics under these conditions.

In Figure 4, it is noted that at $S = 0.5$ cm, the discrepancy in the prediction of liquid-phase velocity among the different turbulence models was negligible, as evidenced by the nearly overlapping curves. The realizable model's curve subtly shifted to the right for $2Z/W > 0$, demonstrating closer alignment with the experimental data. At $S = 5.5$ cm, while there were noticeable variations in how the turbulence models predicted the liquid-phase velocity, these differences were not markedly significant. The standard k-epsilon, RNG, and RSM models produced almost indistinguishable curves, all slightly overestimating the velocity at $2Z/W = 0.25$. Conversely, the SST and realizable models yielded predictions for $2Z/W = 0.25$ that better matched the experimental findings, though they tended to slightly overpredict the velocity at $2Z/W < 0$.

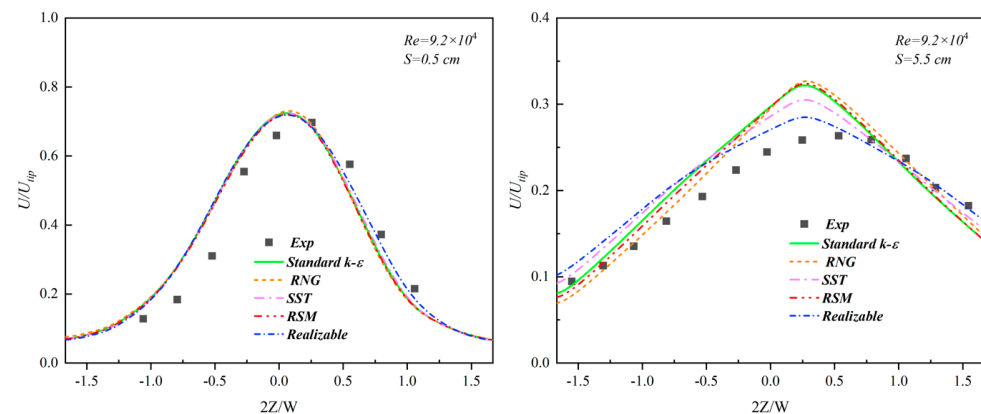


Figure 4. Axial distribution of liquid-phase velocity in the discharge zone under different turbulence models.

Figure 5 showcases the anticipated axial distribution of the gas holdup within the stirred tank, as determined by several turbulence models. Notably, at a distance of 0.5 cm ($S = 0.5$ cm), the realizable model's forecasts for the gas holdup distribution were less precise compared with its counterparts, with the standard k-epsilon model marginally surpassing the other models in terms of accuracy. At a greater distance of 5.5 cm ($S = 5.5$ cm), the predictions made by the RNG model for the gas holdup slightly lagged behind in accuracy, demonstrating only minor discrepancies in comparison with the forecasts from the remaining turbulence models.

Under this study's model conditions, the realizable model offered more accurate predictions for the velocity distribution but was less reliable for gas holdup predictions. Similarly, the RNG model was prone to overestimating the gas holdup, resulting in its early exclusion. Among the other models, the predictions for the velocity distribution were remarkably consistent, yet the standard k-epsilon model excelled at gas holdup predictions and required the least amount of computational resources. Consequently, the standard k-epsilon model was chosen for turbulence modeling.

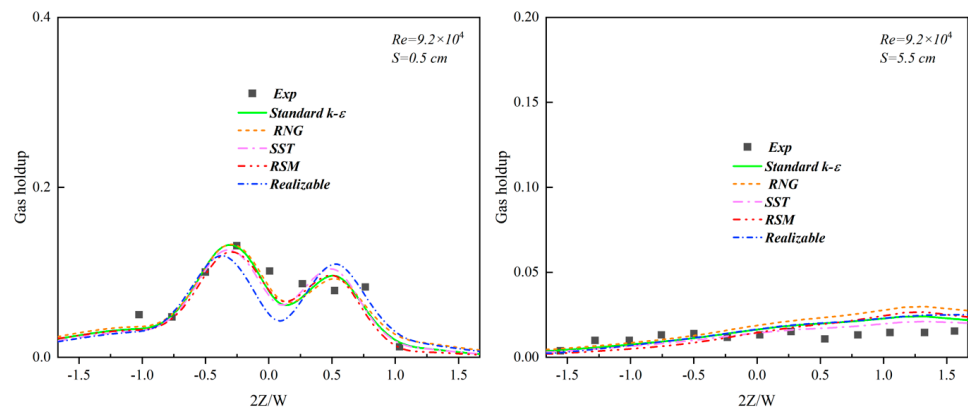


Figure 5. Axial distribution of gas holdups in the drainage area under different turbulence models.

3.3. Drag Force Model Validation

Under gas-liquid two-phase conditions, the study assessed the predictive accuracy of five distinct drag models (Schiller–Naumann, Tomiya, Grace, Ishii–Zuber, and symmetric). This evaluation concentrated on forecasting the axial distribution of the normalized liquid-phase velocity and gas holdup in the discharge area, with a stirring Reynolds number of $Re = 9.2 \times 10^4$ and at proximities of 0.5 cm and 5.5 cm from the impeller tip. The aim was to substantiate the appropriateness of the chosen drag models.

The axial distribution of the liquid-phase velocity, as illustrated in Figure 6 under various drag models, revealed that at $S = 0.5$ cm, the Schiller–Naumann and symmetric models excelled at predicting the velocity distribution compared with the other models. Specifically, the symmetric model tended to overestimate it at $2Z/W = 0$ but delivered superior predictions for $2Z/W > 0$. Conversely, the Schiller–Naumann model, while slightly less accurate than the symmetric model at $2Z/W > 0$, performed marginally better at $2Z/W = 0$. At $S = 5.5$ cm, both the Schiller–Naumann and symmetric models again showed better predictions for the velocity distribution.

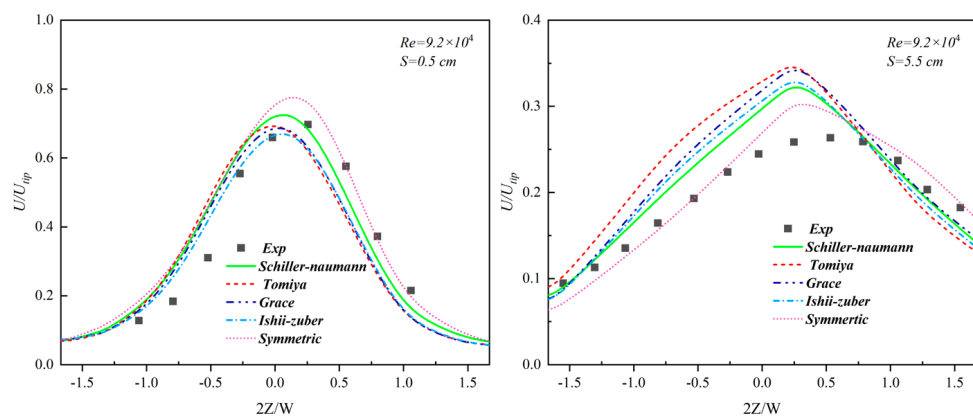


Figure 6. Axial distribution of normalized liquid-phase velocity in the drainage zone under different drag force models.

Figure 7 presents the predicted axial distribution of the gas holdup under different drag models. At $S = 0.5$ cm, the Schiller–Naumann model provided the best prediction for the gas holdup, while the symmetric model offered the worst prediction. At $S = 5.5$ cm, the predictions from the Grace, Tomiya, and Ishii–Zuber models significantly deviated from the experimental values. Among the remaining models, the Schiller–Naumann model performed slightly better than the symmetric model. Among the models evaluated, the Schiller–Naumann model slightly outperformed the symmetric model in terms of accuracy.

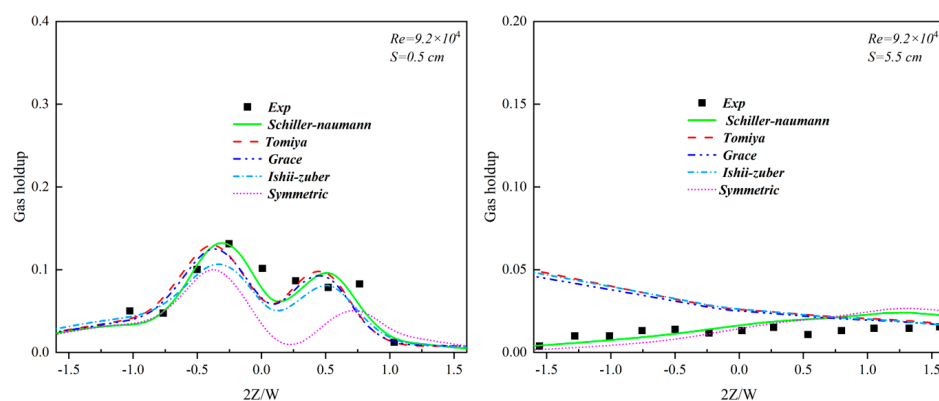


Figure 7. Axial distribution of the gas holdup in the drainage area under different drag force models.

Within the framework of this study's model, the Schiller–Naumann and symmetric models emerged as superior in predicting the velocity distribution. Nevertheless, when focusing on gas holdup prediction, the symmetric model exhibited suboptimal performance at $S = 0.5$ cm in contrast to the Schiller–Naumann model, which demonstrated the most accurate predictions. Consequently, the Schiller–Naumann model was chosen as the preferred drag model.

4. Results and Discussion

4.1. Effect of the Sulfuric Acid Concentration on the Flow Field and Gas Holdup in Stirred Tanks

Sulfuric acid is a commonly used leaching agent in the pressurized leaching process. Too low a concentration of sulfuric acid may result in a low leaching rate, while too high a concentration may result in a waste of resources, and thus the concentration of sulfuric acid is usually discussed in the exploration of the leaching process [33]. In this paper, the effect of the change in physical properties with an increase in the sulfuric acid concentration on the gas-liquid two-phase system in the leaching process was studied through simulations, and the flow field situation in the stirred tank was compared under the three concentration conditions of unadded sulfuric acid solution and common leaching using acidity levels of 60 g/L and 180 g/L. In this paper, under the premise of ensuring computational accuracy and accurately reflecting the flow in the stirred tank, the research object was appropriately simplified to reduce the computational cost. Owing to the relatively low solid content of the slurry in the stirred tank, the solid phase was approximated as the liquid phase. Consequently, the physical phase system in the stirred tank was simplified to a zinc sulfide slurry solution (sulfate solution) and oxygen, with their specific physical phase properties presented in Table 1.

Table 1. Physical parameters of gas-liquid two-phase system in a stirred tank.

Phase	Density ($\text{kg}\cdot\text{m}^{-3}$)	Viscosity [$\text{kg}(\text{m}\cdot\text{s})^{-1}$]
liquid	1500	0.01
gas	1.299	1.919×10^{-5}

The velocity distribution in the stirred tank with different sulfuric acid concentrations is shown in Figure 8, which shows that the addition of sulfuric acid had a significant effect on the flow field in the stirred tank. Compared with the addition of sulfuric acid, the high-velocity region without sulfuric acid was more widely distributed in the stirred tank, and the flow field was also more intense. From the cross-section, it can also be seen that after the addition of sulfuric acid, the velocity near the wall of the stirred tank was significantly reduced, and the high-velocity region after the impeller was also reduced. The alteration of the sulfuric acid concentration from 60 g/L to 180 g/L resulted in a negligible change, with only a minor reduction in the velocity distribution observed. These

phenomena are likely attributable to the increased solution viscosity following the sulfuric acid's addition, enhancing the impeller resistance and the solution's internal friction. In general, the addition of sulfuric acid would reduce the stirring range in the stirred tank, affecting the mixing in the stirred tank, but after a certain concentration of sulfuric acid, and then increasing the concentration of sulfuric acid in the flow field in the stirred tank had less of an effect.

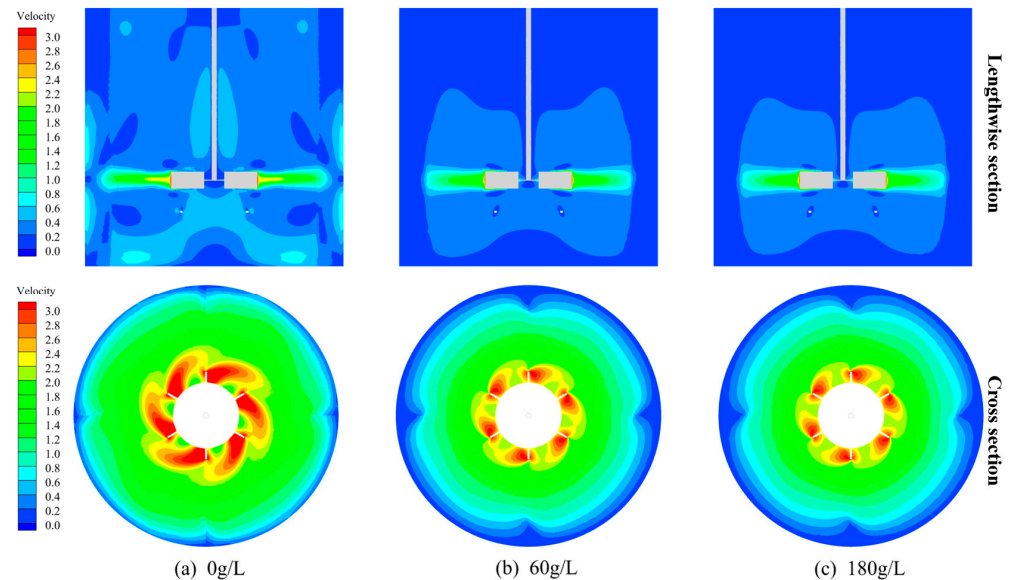


Figure 8. Velocity distribution inside the stirred tank under different concentrations of sulfuric acid.

From the longitudinal section of the cloud diagram of the gas holdup distribution in a stirred tank with different sulfuric acid concentrations in Figure 9, it can be seen that when the sulfuric acid concentration in the stirred tank was 0 g/L, the oxygen distribution area was small. There was a small range of high-content regions. After adding sulfuric acid, the oxygen distribution area increased. Due to the demand for oxygen for the reaction in the tank, the oxygen distribution was more extensive, which was conducive to improving the efficiency of the reaction and increasing the leaching rate. When the sulfuric acid concentration was increased from 60 g/L to 180 g/L, it had less influence on the gas holdup distribution in the stirred tank, and the oxygen distribution only slightly increased.

Combined with the 0.018 contour plot of the gas holdup behind the impeller in the stirred tank with different sulfuric acid concentrations in Figure 10, the gas pockets which formed behind the impeller without adding sulfuric acid were more oversized. Most of the oxygen was concentrated in this region, and the other regions in the stirred tank had lower oxygen contents. After adding sulfuric acid, the cavitation which formed at the back of the impeller was reduced. The gas holdup in other areas of the stirred tank also increased, and the oxygen distribution was more uniform. When the sulfuric acid concentration was increased from 60 g/L to 180 g/L, there was no significant change in the cavitation, and the oxygen distribution in the entire area of the stirred tank slightly increased. Regarding the oxygen content, when the sulfuric acid concentration increased from 0 g/L to 60 g/L, the gas holdup of the stirred tank increased from 0.1944% to 0.2017%, an improvement of 3.75%. In comparison, the gas holdup of the sulfuric acid concentration increased from 0.2017% to 0.2019% when the sulfuric acid concentration increased from 60 g/L to 180 g/L, an improvement of only 0.1%.

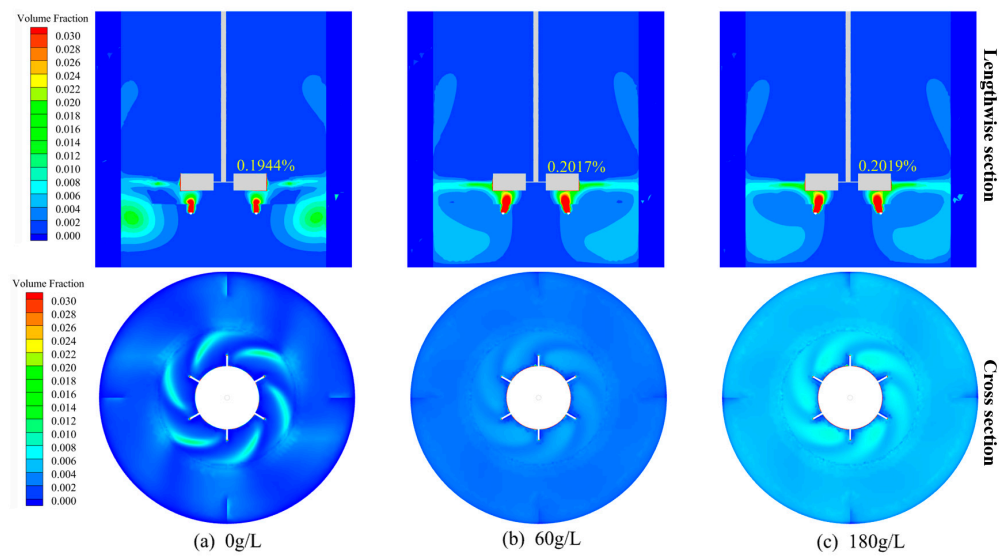


Figure 9. Gas holdup distribution inside the stirred tank under different concentrations of sulfuric acid.

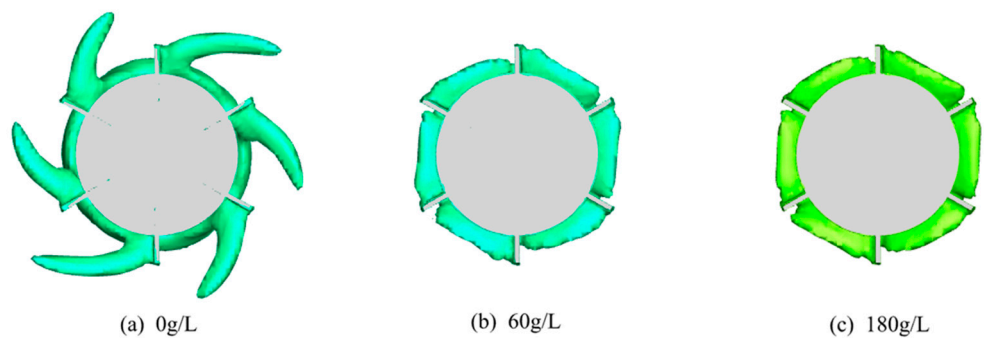


Figure 10. Equivalent plots of 0.018 gas holdup behind the impeller in stirred tanks with different sulfuric acid concentrations.

In general, the increase in the oxygen content may have been due to the addition of sulfuric acid, which led to an increase in the viscosity of the liquid in the stirred tank. The viscosity increase led to the slower rise of the bubbles in the stirred tank, and in the stirred tank, the bubbles increased. Thus, the oxygen content in the stirred tank rose, and the oxygen content was favorable for the reaction in the stirred tank to take place, in addition to reduction of the cavities also being conducive to the gas-liquid mass transfer in the stirred tank.

4.2. Effect of Baffles on the Flow Field and Gas Holdup in the Stirred Tanks

Under the impeller's rotating action, tangential flow around the axis formed in the stirred tank. At high flow rates, the liquid surged toward the tank's wall due to centrifugal force, lowering the central liquid level and forming a vortex. The vortex would inhale the air on the surface, reducing the mixing effect. Usually, the tangential flow is suppressed by adding baffles to improve the impeller's shear performance and the mixing effect. This study installed four baffles with a width of $W/10$ to examine their effect on the gas and liquid phases within the stirred tank, and these baffles were uniformly distributed within the stirred tank, as illustrated in Figure 1a.

Stirring power is an important parameter for stirred tanks, which indicates the power consumption of the stirred tank to a certain extent, and a higher mixing power will cause

energy loss and increased economic costs. The stirring power is calculated by the following formula:

$$P = 2\pi \times T \times \frac{N_r}{60} \quad (9)$$

where P represents the stirring power, N_r denotes the stirring speed, and T signifies the torque, with the torque ascertainable through monitoring calculations. Per the formula, the stirring power with a baffle amounted to 47.31 W, compared with 46.74 W without a baffle, yielding a mere 1.2% difference. It is evident that the inclusion of a baffle results in only a marginal increase in power demand. If the addition of a baffle plate enhances the stirred tank's mixing effect, then from an economic efficiency perspective, it clearly aligns more closely with production requirements.

Figure 11 presents velocity vector diagrams of the stirred tank both with and without the baffle plate, illustrating the fluid motion trends. The observations revealed four "vortices" within the stirred tank. Two circulating structures were identified in the upper and lower sections, aligning with the predictions of the numerical simulations reported in the literature [34]. When there was a baffle, the velocity vector distribution on the cloud diagram was denser, and there was a clear tendency for the velocity vector to be upward in the upper half of the region, which was relative to the presence of a greater axial velocity without a baffle. The axial velocity promotes circulating flow within the stirred tank, favorably enhancing the mixing of the upper and lower flow fields. In the absence of a baffle, the radial velocity at the impeller was slightly higher compared with the scenarios with a baffle due to the lack of obstructions.

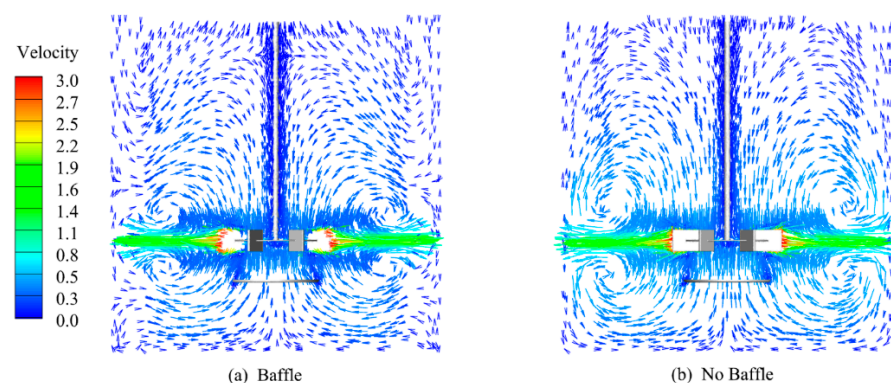


Figure 11. Velocity vector inside the stirred tank with and without baffles.

Figure 12 presents a cloud diagram depicting the gas holdup distribution in the stirred tank, both with and without a baffle, showing that the oxygen distribution areas at the bottom and top of the tank were significantly broader with a baffle. The calculated oxygen content in the stirred tank without a baffle stood at 0.193%, compared with 0.197% in the tank with a baffle, marking a 2% increase in gas holdup. Overall, the inclusion of a baffle modestly enhanced the gas holdup in the stirred tank, beneficially impacting the chemical reactions and thereby improving the leaching rate.

Figure 13 presents a cloud diagram illustrating the velocity distribution in the stirred tank both with and without a baffle. From the longitudinal cross-section, it can be observed that the velocity distribution in the stirred tank without a baffle predominantly concentrated around the impeller plane, forming a confined high-velocity area on both sides of the impeller with a minimal distribution at the top. With the presence of a baffle, the velocity distribution became more widespread, including a notable velocity presence at the top. Introducing a baffle plate expanded the impeller's stirring range, thereby enhancing the stirred tank's mixing efficiency. The cross-sectional velocity distribution cloud diagram reveals a trend where the stirred tank's overall velocity distribution gradually diminished from the center outward. Clearly, the baffle exerted an obstructive effect on the fluid movement, inhibiting the stirred tank's tangential velocity and creating a low-velocity

region behind the baffle, consistent with the phenomena observed in practice. Figure 14 illustrates the axial velocity distribution of the liquid phase in the Y direction at $Z = 0$ in the stirred tank, comparing the scenarios with and without a baffle. The baffle's installation notably enhanced the stirred tank's axial velocity, which benefitted the circulating flow within the tank.

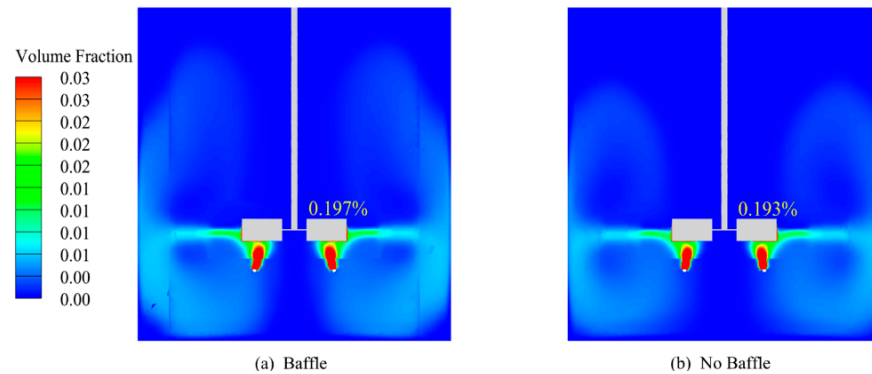


Figure 12. Gas holdup distribution inside the stirred tank with and without baffles.

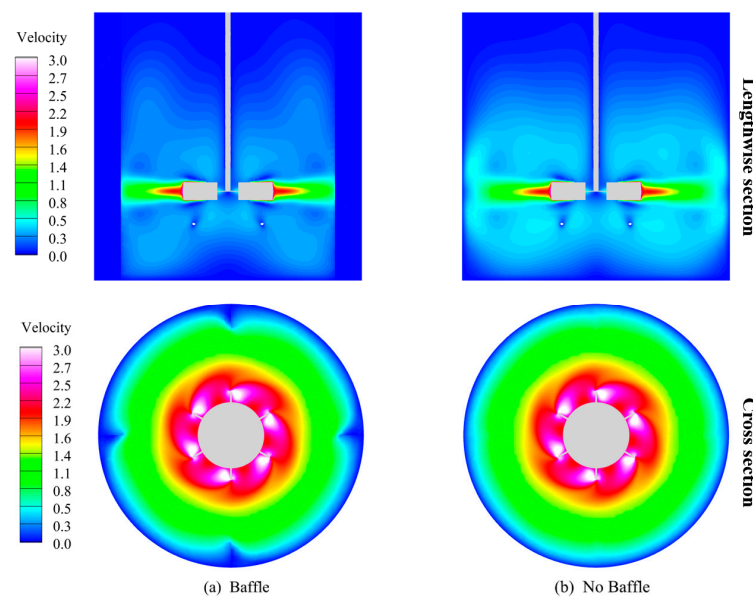


Figure 13. Velocity distribution inside the stirred tank with or without baffles.

Turbulent kinetic energy signifies the magnitude of the vortex energy within the turbulent flow field. Instability of the velocity field precipitates the generation of turbulent kinetic energy. An increase in turbulent kinetic energy indicates enhanced fluid movement speed and irregularity, signifying instability. Numerous energy-intensive turbulence structures, such as vortices and turbines, possessing high velocity and inertia engender a significant perturbation effect on the surrounding flow field, thereby influencing the macroscopic motion and microstructure of the flow field. As depicted in Figure 15, turbulent kinetic energy within the stirred tank primarily concentrated near the impeller. This region was mainly due to the strong rotation of the impeller disrupting the tank flow field to bring about high turbulent kinetic energy. Secondly, for the addition of the baffle plate in the impeller plane of the baffle plate near the emergence of greater turbulent kinetic energy, this was due to the stirred tank's fluid impact in the baffle plate produced by the axial radial speeds, destroying the original flow field structure and generating more turbulent kinetic energy. Turbulent kinetic energy caused by the turbulent structure can increase the

gas-liquid contact area and promote the dissolution of gas. Figure 16 shows that the gas holdup in the stirred tank was improved, while turbulent kinetic energy could also break the limiting structure of the stirred tank so that the quality of the mixing was uniform. Therefore, considering the impact of turbulent kinetic energy, incorporating a baffle plate is beneficial for enhancing the mixing performance and gas content within a stirred tank.

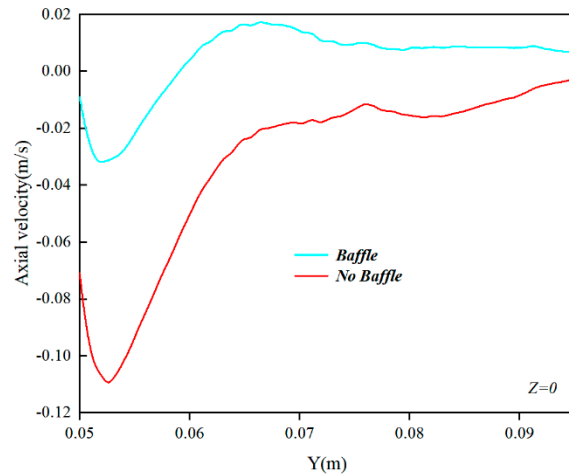


Figure 14. Liquid-phase axial velocity distribution in the Y direction at $Z = 0$ in the stirred tank with or without baffles.

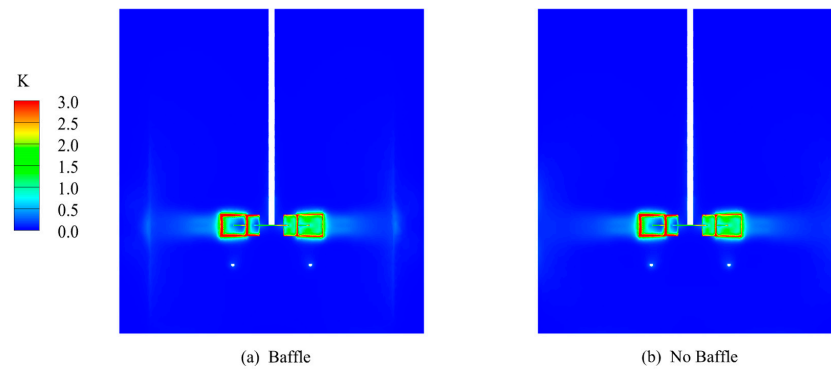


Figure 15. Distribution of turbulent kinetic energy inside the stirred tank with or without baffles.

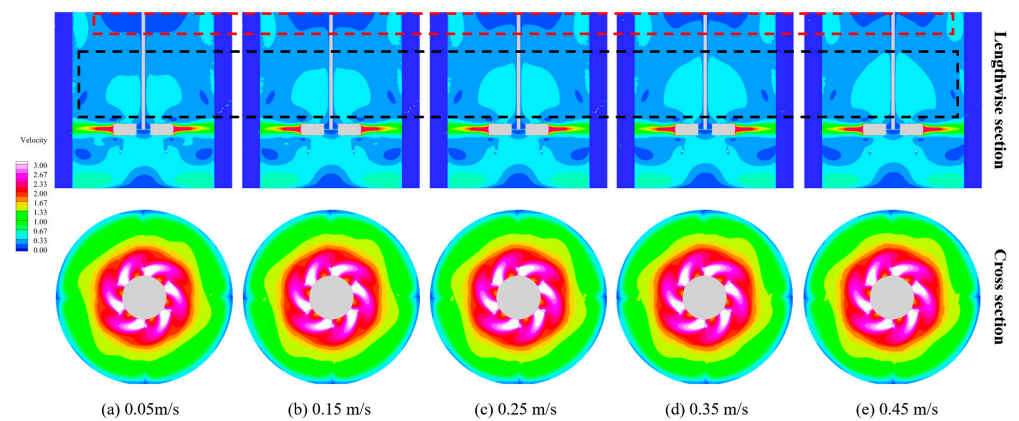


Figure 16. Velocity distribution in the stirred tank at different inlet velocities.

4.3. Influence of the Air Inlet Velocity on the Flow Field and Gas Holdup in Stirred Tanks

This study investigated the impact of five different inlet velocities—0.05 m/s, 0.15 m/s, 0.25 m/s, 0.35 m/s, and 0.45 m/s—on the flow field within a stirred tank. Figure 16 illustrates cloud diagrams of the velocity distribution inside the tank at varying inlet velocities. Viewed from a vertical cross-section, the effect of the inlet velocity on the flow field can predominantly be observed in the upper half of the tank, where the velocity distribution near the stirring shaft increased with a rising inlet velocity. Furthermore, the dead zones at the top of the stirred tank decreased as the inlet velocity increased, suggesting that an increase in the inlet velocity facilitates a more uniform distribution of velocity within the tank. However, from a horizontal cross-section perspective, changes in the inlet velocity did not appear to affect the velocity distribution within the tank, as indicated by the unchanged cloud diagrams. This phenomenon could stem from the relatively high liquid-phase velocity at the plane of the stirring blades, coupled with the insufficient impact of the minimal inlet velocity not significantly altering the liquid flow within the stirred tank. To validate this perspective, the cross-sectional plane at $Z = 0.144$ m was examined, as depicted in Figure 17, where the liquid-phase velocity was comparatively low. The illustration confirms that an increase in the inlet velocity indeed modifies the flow field within the tank.

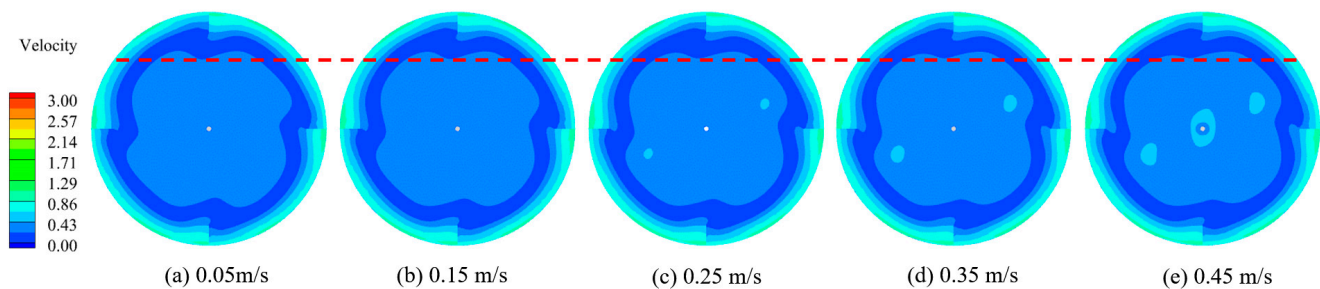


Figure 17. Velocity distribution in the stirred tank at different inlet velocities for $Z = 0.144$ plane.

From the cloud diagrams of the gas holdup distribution within the stirred tank at different inlet velocities shown in Figure 18, it is evident that changing the inlet velocity significantly affected the gas holdup within the tank. With an increase in inlet velocity, the distribution of the gas phase within the tank visibly broadened, and there was a significant increase in the gas holdup. High gas holdup areas were primarily located at the outlets of the annular distributor and the lower half near the tank walls, with less oxygen distributed in the area around the central axis and beneath the impeller blades. From a cross-sectional view, the concentration of oxygen was higher behind the impeller blades. Overall, this was due to the increased inlet velocity leading to a greater volume of gas entering the tank within the same timeframe. Although this resulted in a noticeable increase in the gas holdup within the tank, it also increased oxygen consumption. Therefore, in actual production processes, it is necessary to consider these factors comprehensively to ensure the economic efficiency of production.

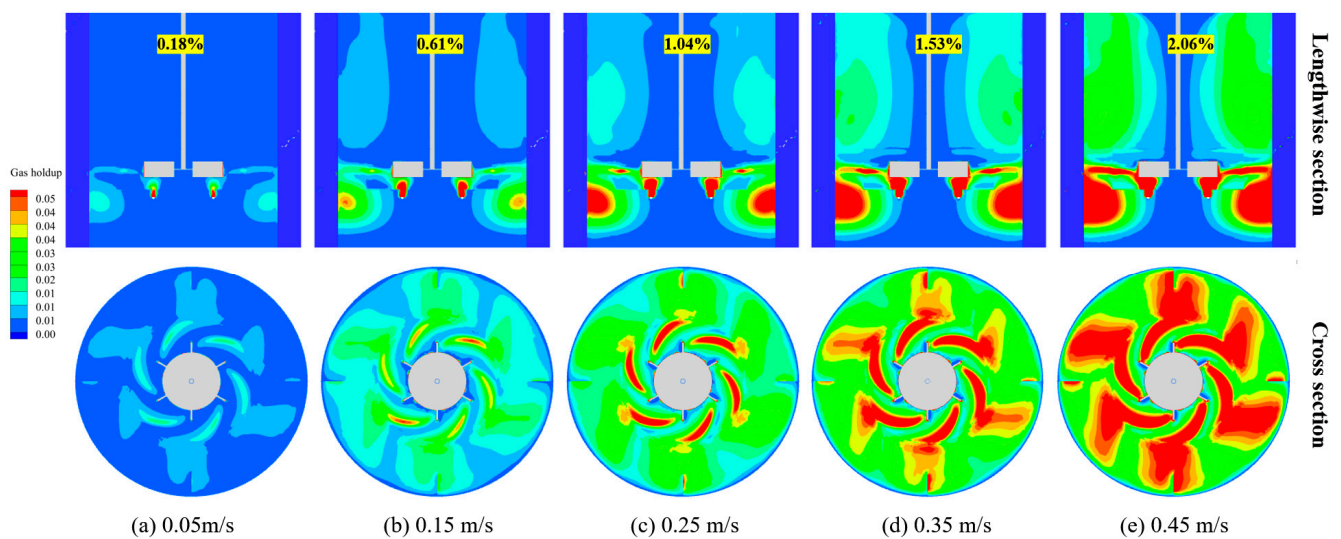


Figure 18. The gas holdup distribution inside the stirred tank at different air inlet velocities.

4.4. Effect of the Bubble Diameter on the Flow Field and Gas Holdup in Stirred Tanks

The influence of three bubble diameters—0.001 m, 0.004 m, and 0.005 m—on the gas-liquid two-phase flow within a stirred tank was investigated. Examination of the velocity distribution cloud diagrams in Figure 19, corresponding to different bubble diameters, revealed that the bubble diameter exerted a minimal impact on the velocity field within the tank, with the velocity distributions being virtually identical across the various bubble diameters. By observing Figure 20, it can be seen that as the bubble diameter increased, the high gas holdup region present after the impeller in the longitudinal section tended to decrease significantly, while in the transverse section, the gas holdup showed a tendency to become more and more widely distributed in the upper half of the distribution and less and less distributed in the lower half of the distribution. This may be because large bubbles receive less resistance and float faster than small bubbles, resulting in a faster gas escape to the liquid surface, and thus the gas holdup distribution increases in the upper half of the region and decreases in the lower half of the area. From the axial velocity distribution of the gas phase in the Y direction at $Z = 0$ in the stirred tank with different bubble diameters in Figure 21, the axial velocity of the gas phase in the stirred tank did increase with the increase in the bubble diameter. At the same time, it was also because of the fast uplift speed of large bubbles that the gas escape increased, leading to a decrease in the total gas holdup in the stirred tank. The overall gas holdup decreased from 1.005% to 0.996% and 0.985% with the increase in inlet bubble size. Although the bubble size impacted the gas holdup in the stirred tank, the effect was minimal.

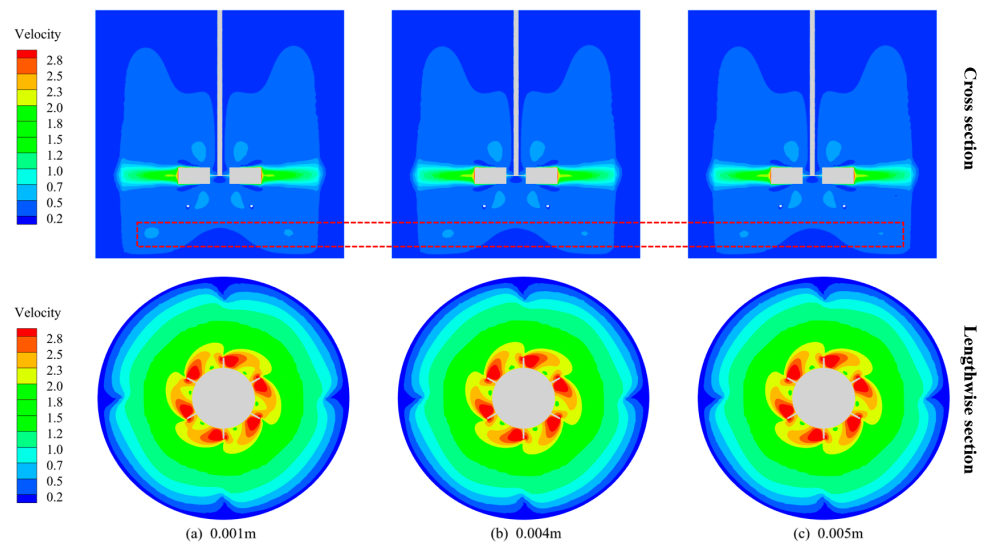


Figure 19. Velocity distribution inside the stirred tank at different bubble diameters.

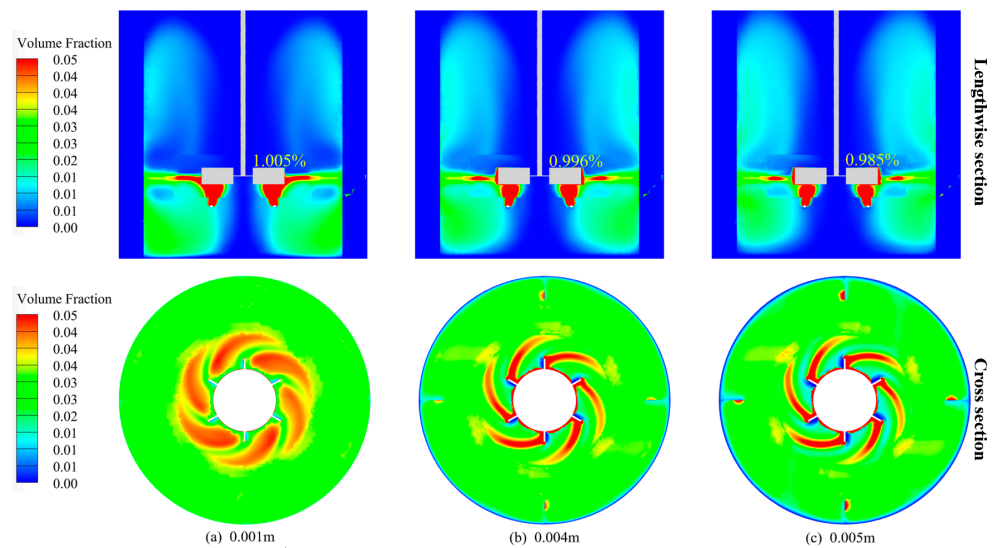


Figure 20. Gas holdup distribution inside the stirred tank at different bubble diameters.

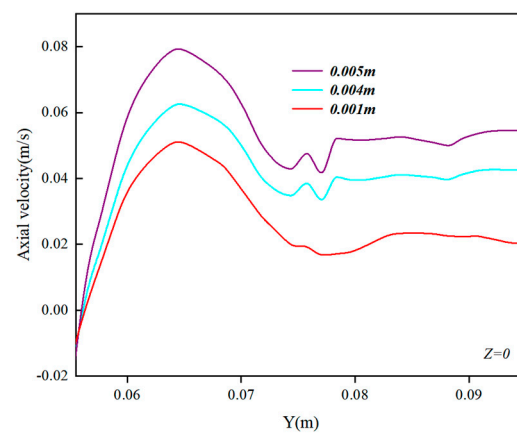


Figure 21. Axial velocity distribution of the gas phase in Y direction at $Z = 0$ in a stirred tank with different bubble diameters.

4.5. Flow Field and Gas Holdup in Stirred Tanks under the Interaction of the Sulfuric Acid Concentration and Inlet Velocity

When observing Figure 22, which depicts the longitudinal section of the stirred tank, it is noticeable that with a sulfuric acid concentration of 180 g/L, the small velocity distribution region beneath the paddles began to diminish as the inlet velocity increased, while the area with a higher velocity distribution in the upper part of the tank tended to expand upward. From the cross-sectional perspective, the velocity cloud remained unchanged. Overall, when comparing the scenarios of sulfuric acid concentrations of 0 g/L and 180 g/L, it was observed that the inlet velocity exerted a reduced impact on the flow field at the higher concentration of 180 g/L.

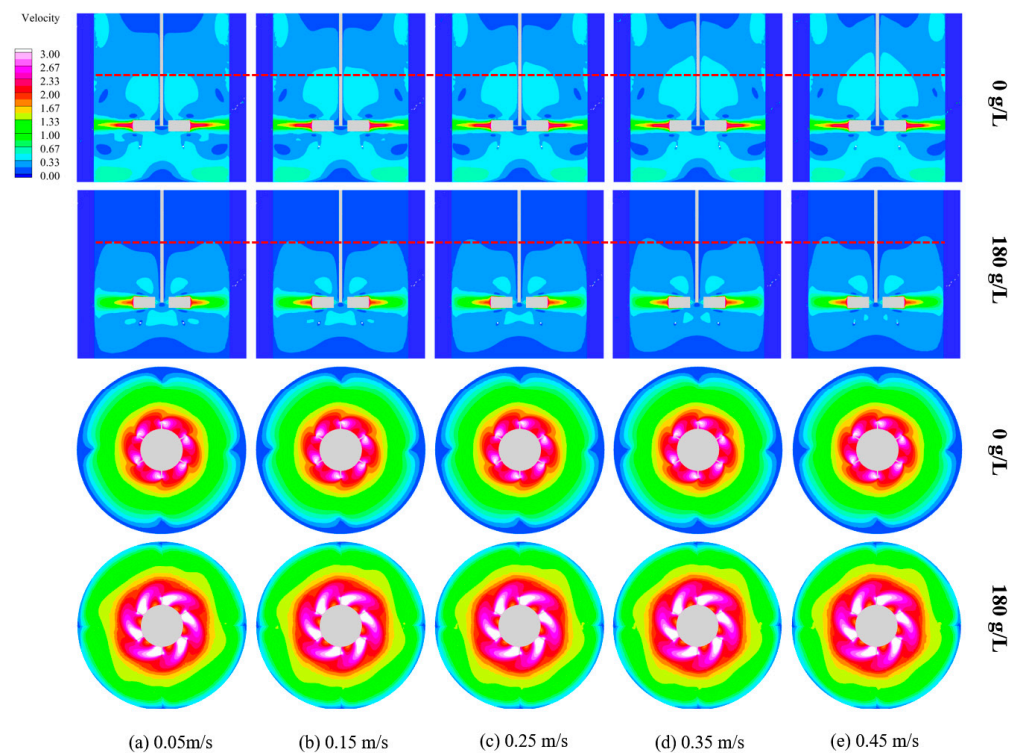


Figure 22. Comparison of velocity distribution clouds for different sulfuric acid concentrations at the same inlet velocity in a stirred tank.

Figure 23 presents a comparison of the gas-phase distributions within the stirred tank across varying inlet velocities and sulfuric acid concentrations. According to the longitudinal section, the gas holdup at a sulfuric acid concentration of 180 g/L exceeded that at 0 g/L by 0.1% when the inlet velocity was set to 0.05 m/s. Conversely, at inlet velocities of 0.15 m/s and 0.25 m/s, the gas holdup at a sulfuric acid concentration of 0 g/L exceeded that at 180 g/L by slight margins of 0.03% and 0.04%, respectively, indicating a minor difference. However, as the inlet velocity increased to 0.35 m/s and 0.45 m/s, the difference became more pronounced, with the gas holdup at a 0 g/L sulfuric acid concentration being 0.17% and 0.32% higher, respectively, than at 180 g/L. Additionally, the gas phase demonstrated a better distribution in the upper half of the stirred tank at a sulfuric acid concentration of 0 g/L. In contrast, at a concentration of 180 g/L, the gas phase occupied a larger and more uniform area in the lower half of the tank.

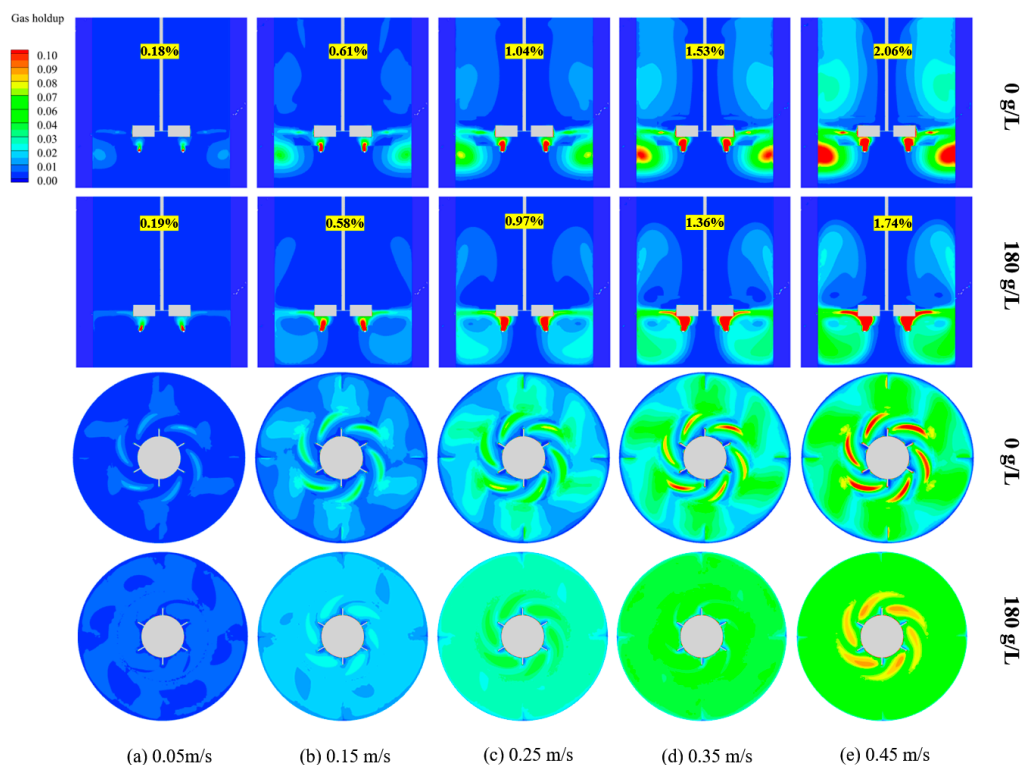


Figure 23. Distribution of gas holdup in stirred tanks with different inlet velocities at different sulfuric acid concentrations.

In the cross-section, the gas-phase distribution was more homogeneous at a sulfuric acid concentration of 180 g/L than at 0 g/L for all inlet velocity conditions.

5. Conclusions

In this study, the finite-volume method was utilized to develop a gas-liquid flow model within a pressurized leaching stirred tank, which was then rigorously validated. The impacts of the sulfuric acid concentration, baffle plate configuration, air inlet velocity, bubble diameter, and other factors on the gas-liquid two-phase dynamics within a sulfuric acid and oxygen system were thoroughly examined, yielding the following key findings:

- (1) The addition of sulfuric acid significantly influenced the gas-liquid dynamics within the stirred tank. At a sulfuric acid concentration of 60 g/L, the velocity of the solution flow decreased, the agitation area was reduced, and the gas holdup increased from 0.1944% to 0.2017%. Further increasing the sulfuric acid concentration to 180 g/L resulted in only a slight increase in the gas holdup from 0.2017% to 0.2019%, with minimal impact on the flow field.
- (2) The installation of baffles in the stirred tank effectively converted the tangential velocity into radial and axial velocities, thus mitigating swirling phenomena. This not only enhanced the distribution of turbulent kinetic energy and promoted mixing within the tank but also resulted in a 2% increase in the gas holdup. Meanwhile, the addition of baffles only increased power consumption by 1.2%.
- (3) Increasing the air inlet velocity had minimal impact on the flow field within the stirred tank, slightly enhancing the velocity distribution and reducing the dead zones at the top of the tank. However, the effect on the oxygen content within the tank was markedly significant, as increasing the inlet velocity from 0.05 m/s to 0.15 m/s, 0.25 m/s, 0.35 m/s, and 0.45 m/s resulted in gas holdup changes of: 0.18%, 0.61%, 1.04%, 1.53%, and 2.06%, respectively.
- (4) Reducing the bubble diameter from 0.005 m to 0.004 m and 0.001 m decreased the axial velocity of the bubbles, thereby increasing the gas holdup time in the tank and

resulting in a gas holdup rate increase from 0.985% to 0.996% and 1.005%, respectively. Consequently, production processes can enhance their gas holdup by reducing the bubble diameter, achieved by decreasing the aperture of the gas distributor or using mixing paddles with greater shear force, among other strategies.

- (5) In further investigations into the interplay between the sulfuric acid concentration and inlet velocity, it was observed that a higher sulfuric acid concentration enhanced the oxygen content in the stirred tank at an inlet velocity of 0.05 m/s. At inlet velocities of 0.15 m/s and 0.25 m/s, a higher sulfuric acid concentration reduced the oxygen content in the tank, and this reduction became more pronounced at gas velocities of 0.35 m/s and 0.45 m/s. This information can serve as a valuable reference for selecting optimal sulfuric acid concentrations and air inlet velocities under specific production conditions.

Ultimately, this study does not completely elucidate the interrelationships among the examined conditions. Subsequent research will endeavor to more thoroughly investigate these interactions.

Author Contributions: Conceptualization, Y.H. and G.X.; methodology, Z.Z. and F.C.; software, Z.Z.; validation, Z.Z., Y.H. and N.Y.; formal analysis, Q.L.; investigation, F.C.; resources, G.X.; data curation, J.L.; writing—original draft preparation, Z.Z.; writing—review and editing, N.Y.; visualization, Z.Z. and F.C.; supervision, N.Y.; project administration, Y.H.; funding acquisition, Y.H. All authors have read and agreed to the published version of the manuscript.

Funding: This work was supported in part by the National Natural Science Foundation of China (Project. Nos. 52074141 and 22168019).

Data Availability Statement: The data presented in this study are available on request from the corresponding author.

Conflicts of Interest: Authors Junchang Liu and Gang Xie are employed by Kunming Metallurgical Research Institute Co., Ltd. The remaining authors declare that the research was conducted in the absence of any commercial or financial relationships that could be construed as a potential conflict of interest.

References

1. Xi, J.; Ji, G.; Liao, Y.; Wu, Y.; Liu, Q.; Li, M. Research on separation and extraction of valuable metals from complex non-ferrous metals resources by high pressure oxygen leaching methodology: A review. *J. Sustain. Metall.* **2022**, *8*, 51–63. [[CrossRef](#)]
2. Liang, M.; Di, H.; Song, L.; Yang, K.; Zhang, L. Study on leaching behaviour of germanium and iron in zinc oxide dust from lead zinc smelting. *Can. Metall. Q.* **2023**, *62*, 573–580. [[CrossRef](#)]
3. Sadeghi, N.; Moghaddam, J.; Ilkhchi, M.O. Kinetics of zinc sulfide concentrate direct leaching in pilot plant scale and development of semi-empirical model. *Trans. Nonferrous Met. Soc. China* **2017**, *27*, 2272–2281. [[CrossRef](#)]
4. Xu, Z.-F.; Jiang, Q.-Z.; Wang, C.-Y. Atmospheric oxygen-rich direct leaching behavior of zinc sulphide concentrate. *Trans. Nonferrous Met. Soc. China* **2013**, *23*, 3780–3787. [[CrossRef](#)]
5. Padilla, R.; Vega, D.; Ruiz, M. Pressure leaching of sulfidized chalcopyrite in sulfuric acid–oxygen media. *Hydrometallurgy* **2007**, *86*, 80–88. [[CrossRef](#)]
6. Tian, L.; Xu, Z.; Chen, L.; Liu, Y.; Zhang, T.-a. Study on oxygen gas holdup and kinetics using various types of paddles during marmatite leaching process. *Hydrometallurgy* **2018**, *180*, 158–171. [[CrossRef](#)]
7. Masterov, M.; Baltussen, M.; Kuipers, J. Numerical simulation of a square bubble column using Detached Eddy Simulation and Euler–Lagrange approach. *Int. J. Multiph. Flow* **2018**, *107*, 275–288. [[CrossRef](#)]
8. Sommer, A.-E.; Rox, H.; Shi, P.; Eckert, K.; Rzehak, R. Solid-liquid flow in stirred tanks: “CFD-grade” experimental investigation. *Chem. Eng. Sci.* **2021**, *245*, 116743. [[CrossRef](#)]
9. Scarano, F. Tomographic PIV: Principles and practice. *Meas. Sci. Technol.* **2012**, *24*, 012001. [[CrossRef](#)]
10. Trindade Koyro, P.; Lima de Moura, H.; de Lima Amaral, R.; Freitas de Lima e Freitas, L.; Duarte Barbutti, A.; Nunhez, J.R.; de Castilho, G.J. Comparison of PIV measurements and OpenFOAM simulations of a stirred tank: Study of the azimuthal position effect. *J. Braz. Soc. Mech. Sci. Eng.* **2022**, *44*, 421. [[CrossRef](#)]
11. Shah, S.; Jain, S.; Patel, R.; Lakhera, V. CFD for centrifugal pumps: A review of the state-of-the-art. *Procedia Eng.* **2013**, *51*, 715–720. [[CrossRef](#)]
12. Zhang, Y.H.; Yong, Y.M.; Mao, Z.S.; Yang, C.; Sun, H.Y.; Wang, H.L. Numerical Simulation of Gas-Liquid Flow in a Stirred Tank with Swirl Modification. *Chem. Eng. Technol.* **2009**, *32*, 1266–1273. [[CrossRef](#)]

13. Wang, S.; Bu, Q.; Luan, D.; Zhang, Y.; Li, L.; Wang, Z.; Shi, W. Study on gas–liquid flow characteristics in stirred tank with dual-impeller based on CFD-PBM coupled model. *Chin. J. Chem. Eng.* **2021**, *38*, 63–75. [[CrossRef](#)]
14. Ochieng, A.; Onyango, M.S.; Kumar, A.; Kiriamiti, K.; Musonge, P. Mixing in a tank stirred by a Rushton turbine at a low clearance. *Chem. Eng. Process. Process Intensif.* **2008**, *47*, 842–851. [[CrossRef](#)]
15. Heidari, A. CFD simulation of impeller shape effect on quality of mixing in two-phase gas–liquid agitated vessel. *Chin. J. Chem. Eng.* **2020**, *28*, 2733–2745. [[CrossRef](#)]
16. Hoseini, S.; Najafi, G.; Ghobadian, B.; Akbarzadeh, A. Impeller shape-optimization of stirred-tank reactor: CFD and fluid structure interaction analyses. *Chem. Eng. J.* **2021**, *413*, 127497. [[CrossRef](#)]
17. Chen, Z.-B.; Yan, H.-J.; Ping, Z.; Ping, Y.; Ding, J.-H.; Jia, L.; Liu, L. Parametric study of gas– liquid two-phase flow field in horizontal stirred tank. *Trans. Nonferrous Met. Soc. China* **2021**, *31*, 1806–1817. [[CrossRef](#)]
18. Naeeni, S.K.; Pakzad, L. Experimental and numerical investigation on mixing of dilute oil in water dispersions in a stirred tank. *Chem. Eng. Res. Des.* **2019**, *147*, 493–509. [[CrossRef](#)]
19. Liangchao, L.; Ning, C.; Kefeng, X.; Beiping, X. A comparative CFD study on gas-liquid dispersion in a stirred tank with low and high gas loadings. *Int. J. Chem. React. Eng.* **2018**, *16*, 20170147. [[CrossRef](#)]
20. Appa, H.; Deglon, D.; Meyer, C. Numerical modelling of hydrodynamics and gas dispersion in an autoclave. *Hydrometallurgy* **2013**, *131*, 67–75. [[CrossRef](#)]
21. Arjunwadkar, S.; Sarvanan, K.; Kulkarni, P.; Pandit, A. Gas-liquid mass transfer in dual impeller bioreactor. *Biochem. Eng. J.* **1998**, *1*, 99–106. [[CrossRef](#)]
22. Zawawi, M.H.; Saleha, A.; Salwa, A.; Hassan, N.; Zahari, N.M.; Ramli, M.Z.; Muda, Z.C. A review: Fundamentals of computational fluid dynamics (CFD). *AIP Conf. Proc.* **2018**, *2030*, 020252.
23. Zhang, H.; Tang, S.; Yue, H.; Wu, K.; Zhu, Y.; Liu, C.; Liang, B.; Li, C. Comparison of computational fluid dynamic simulation of a stirred tank with polyhedral and tetrahedral meshes. *Iran. J. Chem. Chem. Eng. (IJCCE)* **2020**, *39*, 311–319.
24. Panneerselvam, R.; Savithri, S.; Surender, G.D. CFD modeling of gas–liquid–solid mechanically agitated contactor. *Chem. Eng. Res. Des.* **2008**, *86*, 1331–1344. [[CrossRef](#)]
25. Khopkar, A.R.; Ranade, V.V. CFD simulation of gas–liquid stirred vessel: VC, S33, and L33 flow regimes. *AIChE J.* **2006**, *52*, 1654–1672. [[CrossRef](#)]
26. Ljungqvist, M.; Rasmuson, A. Numerical simulation of the two-phase flow in an axially stirred vessel. *Chem. Eng. Res. Des.* **2001**, *79*, 533–546. [[CrossRef](#)]
27. Sanyal, J.; Vásquez, S.; Roy, S.; Dudukovic, M. Numerical simulation of gas–liquid dynamics in cylindrical bubble column reactors. *Chem. Eng. Sci.* **1999**, *54*, 5071–5083. [[CrossRef](#)]
28. Lane, G.; Schwarz, M.; Evans, G. Predicting gas–liquid flow in a mechanically stirred tank. *Appl. Math. Model.* **2002**, *26*, 223–235. [[CrossRef](#)]
29. Coroneo, M.; Montante, G.; Paglianti, A.; Magelli, F. CFD prediction of fluid flow and mixing in stirred tanks: Numerical issues about the RANS simulations. *Comput. Chem. Eng.* **2011**, *35*, 1959–1968. [[CrossRef](#)]
30. Jaworski, Z.; Zakrzewska, B. Modelling of the turbulent wall jet generated by a pitched blade turbine impeller: The effect of turbulence model. *Chem. Eng. Res. Des.* **2002**, *80*, 846–854. [[CrossRef](#)]
31. Bianchi, G.; Rane, S.; Kovacevic, A.; Cipollone, R. Deforming grid generation for numerical simulations of fluid dynamics in sliding vane rotary machines. *Adv. Eng. Softw.* **2017**, *112*, 180–191. [[CrossRef](#)]
32. Guan, X.; Li, X.; Yang, N.; Liu, M. CFD simulation of gas-liquid flow in stirred tanks: Effect of drag models. *Chem. Eng. J.* **2020**, *386*, 121554. [[CrossRef](#)]
33. Whittington, B.; Muir*, D. Pressure acid leaching of nickel laterites: A review. *Miner. Process. Extr. Metallurgy Rev.* **2000**, *21*, 527–599. [[CrossRef](#)]
34. Murthy, B.; Kasundra, R.; Joshi, J. Hollow self-inducing impellers for gas–liquid–solid dispersion: Experimental and computational study. *Chem. Eng. J.* **2008**, *141*, 332–345. [[CrossRef](#)]

Disclaimer/Publisher’s Note: The statements, opinions and data contained in all publications are solely those of the individual author(s) and contributor(s) and not of MDPI and/or the editor(s). MDPI and/or the editor(s) disclaim responsibility for any injury to people or property resulting from any ideas, methods, instructions or products referred to in the content.